Optical Absorption of Silicon Nitride Membranes at 1064 nm and at 1550 nm

Jessica Steinlechner,[1,2] Christoph Krüger,[2] Iain W Martin,[1,*] Angus Bell,[1] Jim Hough,[1] Henning Kaufer,[2] Sheila Rowan,[1] Roman Schnabel,[2,3] and Sebastian Steinlechner[1,2]

[1] *SUPA, School of Physics and Astronomy, University of Glasgow, Glasgow, G12 8QQ, Scotland*
[2] *Institut für Gravitationsphysik, Leibniz Universität Hannover and Max-Planck-Institut für Gravitationsphysik (Albert-Einstein-Institut), Callinstr. 38, 30167 Hannover, Germany*
[3] *Institut für Laserphysik and Zentrum für Optische Quantentechnologien, Universität Hamburg, Luruper Chaussee 149, 22761 Hamburg, Germany*

Due to a low mechanical loss, thin films made of silicon nitride (Si_3N_4) are interesting for fundamental research and development in the field of gravitational-wave detection. Si_3N_4-membranes allow for the characterization of quantum radiation pressure noise (RPN), which will be a limiting noise source in gravitational-wave detectors of the 2nd and 3rd generation. Furthermore, Si_3N_4 is an interesting material for possible thermal noise reduction in highly-reflective mirror coatings. For both applications, the optical absorption of Si_3N_4 needs to be low. This paper presents absorption measurements on low-stress Si_3N_4 membranes showing an absorption a factor of seven lower at 1550 nm than at 1064 nm resulting in an estimated two-times higher sensitivity in RPN experiments at the higher wavelength and making Si_3N_4 an interesting material for highly-reflective multi-material mirror coatings at 1550 nm.

I. INTRODUCTION

On 14th of September 2015 the first gravitational wave (GW) signal was observed by the Advanced LIGO GW detectors [1] – one hundred years after having been predicted by Einstein in his general theory of relativity. To make GW detection possible, over the past decades large-scale Michelson interferometers with arm lengths of up to 4 km have been developed, using laser interferometry to measure changes in the relative separation of suspended and highly-reflective coated test-masses.

Once the Advanced LIGO generation of GW detectors reaches its design sensitivity, it is expected to be limited by radiation pressure noise (RPN) at frequencies below ≈ 40 Hz [2]. While up to now the occurrence of RPN in GW detectors is merely a theoretical prediction, RPN has been measured in a cryogenic cavity setup using a nanogram membrane oscillator [3]. Various experiments aiming to measure and characterize this noise source are in progress [4–7].

One option to measure RPN is a Michelson-Sagnac interferometer using a translucent silicon nitride (Si_3N_4) membrane with sub-wavelength thickness [6] such as shown in Fig. 1. Heating of the membrane induced by optical absorption limits quantum opto-mechanical experiments at low temperatures. In [6] the absorption of Si_3N_4 membranes of different thickness is calculated, accounting for beam geometry effects, based on an imaginary part of the refractive index of $k = 1.5 \times 10^{-4}$ at a laser wavelength of 1064 nm [8]. A change in wavelength is an option to reduce absorption and resulting heating of the membrane.

Thermal noise is a second noise source for which the absorption of Si_3N_4 is of interest. Advanced LIGO, upgrades to Advanced LIGO [9], and future detectors such as the low frequency detector of the *Einstein Telescope* (ET) [10, 11] will be limited by thermal noise in the most sensitive part of the detection band. To reduce thermal noise, these detectors may be operated at cryogenic temperatures, which requires a change of the test-mass material as the currently used material, fused silica, has a high mechanical loss at low temperature resulting in a net increase in thermal noise due to cooling [12]. Crystalline silicon (cSi) is a possible test-mass material showing low mechanical loss at low temperatures [13], but it is not transparent at the currently used laser wavelength of 1064 nm. Consequently, use of a higher wavelength of 1550 nm or even 2000 nm, at which cSi shows lower absorption, has been proposed [10, 14].

Present highly-reflective mirror coatings are made of silica (SiO_2) and titania-doped tantala (Ti:Ta_2O_5). The mechanical loss of the coatings at low temperatures has to be reduced to match the thermal noise requirements of future GW detectors. Therefore new materials have to be developed which show suitable mechanical properties while meeting challenging requirements on reflectivity and optical absorption [10].

Si_3N_4 is an interesting material for low thermal noise highly reflective mirror coatings, with a mechanical loss in the order of $\phi = 10^{-5}$ at 20 K for a coating on a substrate [21] and $< 10^{-6}$ for highly stressed substrate-free thin films [22]. This is significantly lower than the mechanical loss of SiO_2 ($\phi = 7.8 \times 10^{-4}$ at 20 K [35]) and Ti:Ta_2O_5 ($\phi = 8.6 \times 10^{-4}$ at 20 K [16]). Si_3N_4 may be of particular interest for use in multimaterial designs [19, 20], in which more than two materials are combined to simultaneously exploit optical and mechanical properties optimally. In these designs, materials with low mechanical loss, but high optical absorption are used in lower coating layers, in which the laser power is reduced, to keep the total absorption low. The lower the absorption, the closer to the top of the coating a material

* iain.martin@glasgow.ac.uk

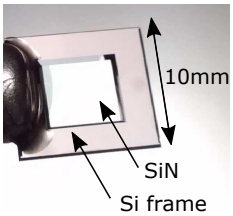

FIG. 1. Photo of a LPCVD Si_3N_4 membrane fabricated by Norcada [26]: A silicon substrate was coated with Si_3N_4 and a 5 mm × 5 mm window was etched into the silicon substrate to produce the Si_3N_4 membrane.

refractive index n at 1550 nm	2.17 [26]
coefficient of thermal expansion $a_{\rm th}$	$(2.6 \pm 1.1) \times 10^{-6}\,{\rm K}^{-1}$ [25]
thermo refractive coefficient ${\rm d}n/{\rm d}T$	$4 \times 10^{-5}\,{\rm K}^{-1}$ [24]
density ρ	$3100\,{\rm kg/m}^3$ [26]
heat capacity c	$(523.2 \pm 78.5)\,{\rm J/(kgK)}$ [27]
thermal conductivity $k_{\rm th}$	$(4.9 \pm 0.7)\,{\rm W/(mK)}$ [27]

TABLE I. Material parameters of Si_3N_4 which were used for simulating the PCI signal

can be used.

Investigations of silicon nitride deposited via plasma-enhanced chemical vapor deposition (PECVD) also show significant promise, with evidence of lower mechanical losses than current GW coating materials at room temperature and at low temperature down to 10 K [17, 18]. The refractive index of this material varies with the precise composition, leading to the interesting possibility of using silicon nitride layers of different composition for both the high and low index parts of an optical coating.

This paper presents absorption measurements on amorphous Si_3N_4 membranes manufactured by *Norcada* [26] via low-pressure chemical vapor deposition (LPCVD), which is the same deposition method as investigated in [21]. Both low-stress membranes (≤ 250 MPa) and high-stress membranes (800 MPa) are available, but only the low-stress membranes had a suitable thickness for optical absorption measurements, and therefore were used for the studies presented here. There is evidence that stress in the order of 1 GPa [22] can significantly reduce the mechanical loss of substrate-free silicon nitride films deposited by PECVD. It would be of interest to investigate if higher stress can also affect the optical absorption of silicon nitride.

Figure 1 shows a photo of a Si_3N_4 membrane such as used in our measurements: Photothermal common-path interferometry (PCI) [23] was used for thermally based absorption measurements at 1550 nm and at 1064 nm on a membrane 2 μm in thickness. Cavity round-trip loss measurements were used to provide an upper limit for the absorption of membranes 1 μm, 100 nm, and 50 nm in thickness. The consequences of the absorption results for RPN experiments and for coating thermal noise are discussed.

II. OPTICAL ABSORPTION MEASUREMENTS USING PCI

In this section, thermal-based absorption measurements at 1550 nm and at 1064 nm, using photothermal common-path interferometry (PCI) [23], on a membrane 2 μm in thickness are presented.

The PCI technique uses a strong pump laser beam with small waist to create a thermally induced optical length change in a substrate due to optical absorption. The pump beam is crossed by a weak probe beam that has a larger diameter. The portion of the probe beam overlapping the pump is affected by the optical length change resulting in a phase shift. The phase-shifted and non phase-shifted portions of the probe beam interfere. This interference has a maximum value when measured approximately one (probe) Rayleigh range from the probe waist. The interferometric phase change measured at this point is directly proportional to the absorption of the material and is calibrated using a fused silica substrate with known absorption. Based on the thermal diffusivity of the materials, an additional scaling factor of 0.57 is used to scale the amplitude signal from Si_3N_4 to the signal from the fused silica calibration substrate [23].

Amplitude modulation of the pump beam provides information of the phase of the signal with reference to the pump modulation. This phase is determined by the thermal diffusion of the material and the geometric parameters of the pump beam and provides an additional consistency check for the measured absorption signal. The phase response of Si_3N_4 to the amplitude modulation frequency of 407 Hz used in the experiment, based on the material parameters listed in Tab. I is expected to be $(-40 \pm 6)^\circ$. The error bars result from the errors given for the literature values for c and $k_{\rm th}$ [27].

Etalon effects occur in the Si_3N_4 membranes. Figure 2(a) shows the reflectivity for a membrane 2 μm in thickness at the probe-laser wavelength of 1620 nm depending on the angle of incidence. At an angle of 51°, in which case the light field within the membrane is on resonance, all laser light is transmitted by the membrane. Independent of the membrane geometric parameters, Brewster's angle for p-polarized light (pump beam, 1550 nm) is at $\arctan(n_{\rm Si_3N_4}) = 65\,^\circ$. A crossing angle of pump and probe beam of 14° therefore can provide total transmission for both beams simultaneously, as shown in Fig. 2(b).

Figure 2(c) shows a typical absorption measurement using PCI taken on the 2 μm membrane at a wavelength of 1550 nm. The purple line shows the absorption signal (left y axis), and the green line shows the phase response (right y axis) for scanning the position of the membrane through the beam crossing point at which the absorption signal maximizes to 226 ppm. The width of the main peak results from the spatial resolution of the technique, the small side maxima are interference fringes characteristic for PCI. The corresponding phase of $-42\,^\circ$ is in agreement with the theoretical prediction. The absorption is given per effective membrane thickness $t_{\rm M}$ at Brewster's angle $\Theta_{\rm B}$ considering the laser beam transmitting the membrane at an an-

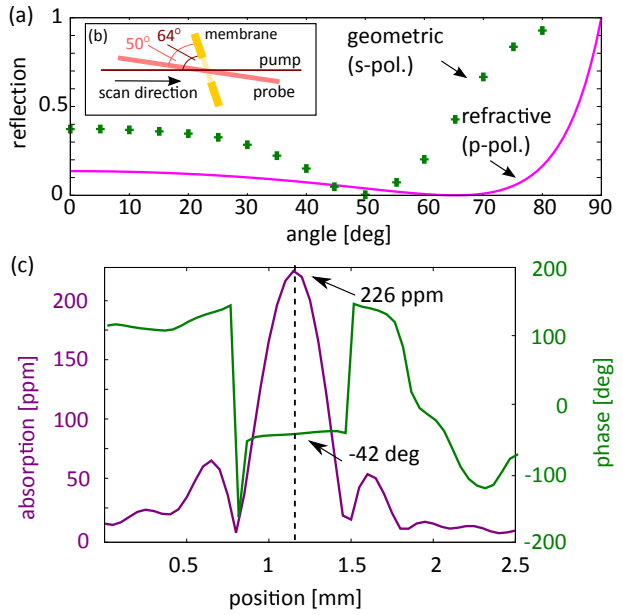

FIG. 2. (a) Brewster's angle for Si_3N_4 is at 65 ° (minimum of pink line), independent from the thickness of the substrate. At this angle the p-polarized pump light is transmitted. Due to an etalon effect, the 2 μm thick Si_3N_4 membrane transmits most of the incident laser power at an angle of incidence of 50 °, at which the s-polarized probe light is transmitted. (b) Probe beam (1620 nm) and pump beam (1550 nm/1064 nm) are crossing at an angle of about 14 ° inside the membrane. (c) Typical absorption measurement at 1550 nm using PCI. Absorption signal (purple): The membrane position is scanned along the direction of the pump beam and reaches a maximum of 226 ppm in the beam crossing point. Phase signal (green): The phase response to the amplitude modulation of the pump beam is −42 °.

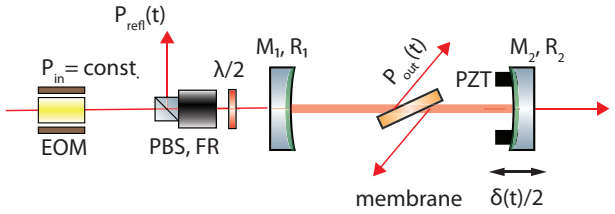

FIG. 3. Experimental setup for indirect absorption measurements via cavity round-trip loss: The membrane was positioned at Brewster's angle inside the cavity to minimize loss P_{out} due to reflected light.The cavity length was periodically modulated and resulting cavity resonance peaks were detected using a photo diode in reflection, the signal being separated from the incident beam with a faraday rotator (FR).

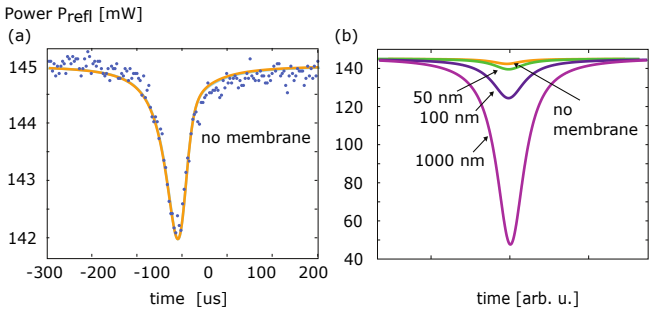

FIG. 4. (a) Reflected resonance peaks at 1064 nm without membrane: measured peak: blue dots, simulated peak: orange line. (b) Fitted resonance peaks for the cavity without membrane (orange line), and for membranes different in thickness. The impedance mismatch of the overcoupled cavity decreases with increasing absorption loss due to increasing membrane thickness.

gle $(90° - \Theta_B)$. This effective transmission length of $t_M = t \times \cos(90° - \Theta_B) = 1.1 \times t = 2.2\,\mu$m results in an absorption coefficient of $\alpha = 1.03\,\mathrm{cm}^{-1}$. The mean value for the absorption of ten measurements taken at different positions on the membrane is 213 ppm with a standard deviation of 17 ppm. At 1064 nm, five measurements showed an average absorption of 1512 ppm with a standard deviation of 27 ppm.

During the measurements, the calibration was routinely checked. For a change of more than 10 % due to misalignment (mechanical drift of mirror mounts mainly), measurements were repeated. Since this 10 % error dominates the standard deviation, errors from power meter uncertainties, laser power fluctuations during a measurement, and discrepancies of the results after realignment, for all measurements a maximum error of ±10 % is assumed. This results in an absorption coefficient of $(1.0 \pm 0.1)\,\mathrm{cm}^{-1}$ at 1550 nm and $(6.9 \pm 0.7)\,\mathrm{cm}^{-1}$ at 1064 nm. The absorption reduces by factor of 7 at a wavelength of 1550 nm compared to 1064 nm. Material properties for silicon nitride in literature vary strongly. Errors from such uncertainties can additionally affect our absorption results while not being relevant for the absorption ratio at the two wavelengths.

Measuring membranes 500 nm and 1000 nm in thickness using the PCI technique, resulted in phase values of about 120° instead of -42°. A phase differing significantly from the prediction indicates an invalid absorption result. The angle of total transmission for the probe beam shown in Fig 2a (green crosses) is a geometric effect, which only exists for the 2000 nm thick membrane, but not for the thinner membranes available, and the phase only agrees with the theory at this angle. A more detailed explanation can be found in the Appendix.

III. CAVITY ROUND TRIP LOSS MEASUREMENTS

The optical absorption of thinner membranes, which we were unable to measure using the PCI technique, was indirectly measured via roundtrip loss in a Fabry Perot cavity. This allowed measurements of membranes closer in thickness to those typically used for RPN experiments, and measurements of absorption versus thickness pro-

vided a useful cross-check of our PCI result for the 2 μm thick membrane.

Figure 3 shows a schematic of the experimental setup. The cavity was formed by an input mirror M_1 with design reflectivity $R_{1,1064\mathrm{nm}} = 99\,\%$ ($R_{1,1550\mathrm{nm}} = 99.4\,\%$) and a highly-reflective (HR) coated end mirror M_2, which were fixed to an aluminium spacer at a distance of $L_{1064\mathrm{nm}} = 158\,\mathrm{mm}$ ($L_{1550\mathrm{nm}} = 163\,\mathrm{mm}$). A membrane was positioned in the cavity at Brewster's angle. The cavity length was varied using a piezo-electric transducer (PZT) fixed between the end mirror and the spacer. At resonance, $L = n \times \lambda/2$, a peak in transmitted power and a corresponding minimum in reflection occurs. The cavity length was scanned only around the resonance (for details see end of this section). A polarizing beam splitter (PBS) and a Faraday rotator (FR) separated the reflected light field P_{refl} from the incoming light field P_{in}. The reflected resonance peak of the cavity was measured with a photo diode. The $\lambda/2$-waveplate was used to match the polarization of the laser light inside the cavity to Brewster's angle of the membrane. The electro-optical modulator (EOM) imprinted sidebands onto the light field to calibrate the motion of the end mirror.

The cavity round-trip loss caused by the membranes was measured in two steps. In the first step, resonance peaks without a membrane were detected to characterize cavity properties such as the reflectivity R_1 of M_1 and the effective out-coupling reflectivity $\widetilde{R}_2$, with $\widetilde{R}_2$ including the absorption and scattering losses of M_1 and M_2. The cavity was designed to be impedance mismatched ($\widetilde{R}_2 \gg R_1$) and therefore only small resonance peaks formed (impedance matching $\approx 2\,\%$). Figure 4(a) shows a measurement of a resonance peak of the cavity for 1064 nm without membrane (blue dots). The orange line is a fit to the measurements using R_1 and $\widetilde{R}_2$ for fit parameters as described in [28]. The resulting cavity parameters (mean value and standard error) are $R_1 = (98.916 \pm 0.004)\,\%$ and a round-trip loss of $1 - \widetilde{R}_2 = (49 \pm 1)\,\mathrm{ppm}$, which corresponds to a finesse of $F = 574$. These results are an average number taken from 14 measurements. At 1550 nm the loss of the cavity was measured from 10 single measurements. The result was $R_1 = (99.428 \pm 0.003)\,\%$ and $1 - \tilde{R}_2 = (100 \pm 1)\,\mathrm{ppm}$, with a finesse of $F = 1078$.

In the second step, a membrane was placed inside the cavity. Loss caused by the membrane effectively decreased the reflectivity $\widetilde{R}_2$ (while R_1 stayed constant) and therefore the impedance mismatch. Figure 4(b) shows fitted resonance peaks for the cavity at 1064 nm without membrane (orange line, identical to 4(a)) and with membranes 50, 100 and 1000 nm in thickness. The alignment of the membrane to Brewster's angle was optimized by rotating both the wave plate and the membrane, minimizing the round-trip loss. Detecting and fitting the resonance peaks provided information of the loss caused by the membrane including surface scattering and reflection loss. The remaining power P_{out} reflected at the membrane surface at resonance was measured with a calibrated photo diode. The procedure was repeated for different membranes placed in the cavity. For each membrane, R_1 and $\tilde{R}_2$ were fitted and are given in Tab. II. Between 10 and 14 single measurements varying the cavity length-scan frequency were performed for each of 5 membranes at 1064 nm and 6 membranes at 1550 nm. Due to the incident light being at Brewster's angle the path through the membrane t_{M} is longer by a factor of 1.1 than the path under normal incidence.

The single pass absorption of a membrane at Brewster's angle can be calculated from

$$\alpha = \left(\frac{\tilde{R}_2 - \tilde{R}_{2\mathrm{mem}}}{2} - \frac{P_{\mathrm{out}}}{P} \right) \times \frac{1}{t_{\mathrm{M}}} \,. \qquad (1)$$

$\tilde{R}_2 - \tilde{R}_{2\mathrm{mem}}$ gives the cavity round trip loss caused by the membrane normalized to the input power, which is divided by 2 to take into account passing the membrane twice per round trip. The normalized power reflected due to non-perfect alignment of the membrane to Brewster's angle is subtracted from the round trip loss. The remaining loss per effective membrane thickness at Brewster's angle is divided by a factor of 1.1 to calculate the loss per membrane thickness. Table II gives the absorption coefficient α normalized to cm^{-1} for all membranes.

Figure 5 shows the absorption results taken on the different membranes compared to the prediction made in [6] based on $k = 1.5 \times 10^{-4}$ [8]. Due to the use of Brewster's angle in our experiments the membrane could not be placed within a node or anti-node of the standing-wave light field inside the cavity, but the absorption originated from an integration over many nodes and anti-nodes represented by the pink line. The black dots represent the experimental results from the cavity measurements at 1064 nm and the green triangles results at 1550 nm. The two measurements furthest to the right for a membrane thickness of 2 μm were taken with the PCI (blue dot: 1064 nm, purple triangle: 1550 nm).

While an increasing trend of the absorption with membrane thickness as expected is clearly visible for both wavelengths, the cavity results are very scattered, which most likely was caused by surface effects as the setup is very sensitive to non-perfect alignment. The lower results of the cavity measurements confirm the PCI measurements, which is indicated by the red dashed line for 1064 nm and by the orange dotted line for 1550 nm. For further discussion in this paper the results obtained with the PCI are used as they were the only actual measurement of absorption, while the cavity measurements only provided upper limits on the absorption.

The standard error of the fits of the individual resonance peaks is very small. However, additional uncertainty is introduced through the calibration of the mirror motion (corresponding to the time axis in 4), and this dominates the final error in the measurements. For the calibration, sidebands converted into a Pound Drever

Membrane	No. of meas.	R_1 [%]	P_{out}/P [ppm]	$(1-\tilde{R}_2)$ [ppm]	α [cm^{-1}]	No. of meas.	R_1 [%]	P_{out}/P [ppm]	$(1-\tilde{R}_2)$ [ppm]	α [cm^{-1}]
	1064 nm					1550 nm				
-	14	98.916 ± 0.004	-	49 ± 1	-	10	99.428 ± 0.003	-	100 ± 1	-
50 nm 1	13	98.922 ± 0.003	< 1	100 ± 1	4.7 ± 0.2	10	99.411 ± 0.002	1	121 ± 1	1.8 ± 0.02
50 nm 2	13	98.941 ± 0.004	1	123 ± 1	6.5 ± 0.2	9	99.410 ± 0.007	1	243 ± 5	12.9 ± 0.05
100 nm 1	10	98.896 ± 0.009	5	234 ± 3	8.0 ± 0.2	10	99.421 ± 0.011	2	138 ± 2	1.5 ± 0.01
100 nm 2						9	99.416 ± 0.003	1	128 ± 1	1.2 ± 0.01
100 nm 3	12	98.920 ± 0.005	1	486 ± 2	19.8 ± 0.3					
1000 nm 2	12	98.928 ± 0.003	4	3155 ± 10	14.4 ± 0.1	10	99.410 ± 0.004	5	2115 ± 13	9.1 ± 0.01
1000 nm 3						10	99.422 ± 0.002	3	380 ± 2	1.3 ± 0.001

TABLE II. Results for R_1 and $(1-\tilde{R}_2)$ at 1064 nm and 1550 nm for different membranes and without membrane. The number of single measurements varying per series is given as well as the power P_{out} reflected at the membrane surface due to non perfect Brewster's angle. The resulting absorption coefficient is normalized to cm^{-1}.

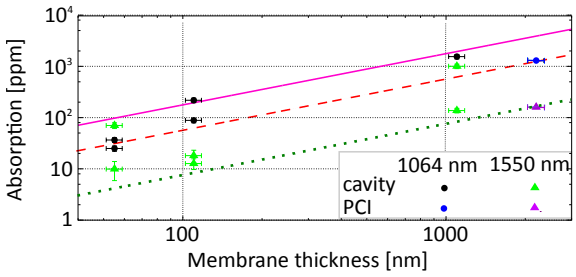

FIG. 5. The pink line shows the prediction of the absorption at 1064 nm made in [6] based on $k = 1.5 \times 10^{-4}$ [8]. Geometric effects associated with the position of the membrane relative to standing wave nodes or anti nodes in the cavity are not relevant in our case due to the use of Brewster's angle. The black dots present the experimental results from the cavity measurements work at 1064 nm and the green triangle results at 1550 nm. The results from the PCI measurements are shown by the blue dot (1064 nm) and the purple triangle (1550 nm). The dashed red and dotted green lines extrapolate the PCI results indicating a lower limit for the absorption.

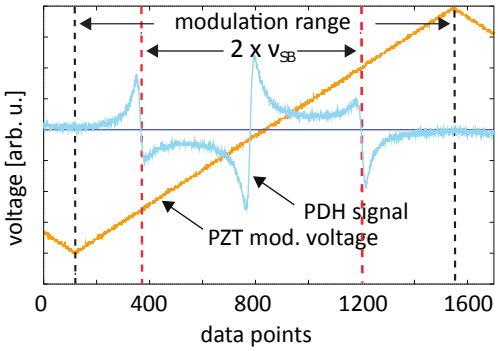

FIG. 6. Example for a measurement of N_{FSR}: The yellow curve shows the PZT modulation voltage (= ramp signal), the light blue curve shows a PDH signal. The ratio of the modulation range (black dashed lines) and the separation of the side bands (= 2× the sideband frequency ν_{SB}, red dashed lines) multiplied with the sideband separation and divided by the free spectral range (FSR) of the cavity provides the number of free spectral ranges N_{FSR} scanned per ramp side.

Hall (PDH) signal [29] were used such as shown by the blue line in Fig. 6. This signal results from a side band frequency ν_{SB}. The separation of the side bands which are positioned at the zero-crossings of the PDH signal are marked by the red dashed lines. The modulation voltage following a triangular ramp function is shown in yellow with a modulation range marked by the black dashed lines. In Fig. 6 the ratio of modulation range (black lines) and side band separation (red lines) is $R \approx 2$. The number of free spectral ranges N_{FSR} scanned per ramp is then given by

$$N_{FSR} = R \times \frac{2 \times \nu_{SB}}{\nu_{FSR}}, \qquad (2)$$

where ν_{FSR} is the free spectral range of the cavity.

For measurements at 1064 nm, N_{FSR} was between 0.07 and 0.08, and about 0.04 at 1550 nm. N_{FSR} was determined for each measurement. The value slightly increased with scan frequency. This measurement is very accurate and the total error of the measurements is given by the standard error of the results in Tab. II.

IV. DISCUSSION

A. Relevance for RPN experiments

The thermal noise (power) spectral density is a limiting factor for reaching the RPN dominated regime in membrane experiments. It is directly proportional to the temperature of the membrane T_{mem} [30]. The temperature of the membrane in such experiments in turn is usually fully defined by the absorption of laser light. The optical absorption of membranes presumably depends on the temperature. Making the assumption that the ratio of the absorption coefficients $\alpha_{1064}/\alpha_{1550} \approx 7$ is only moderately temperature dependent, a change in wavelength from 1064 nm to 1550 nm in RPN experiments based on membranes should allow the use of 7× higher laser power

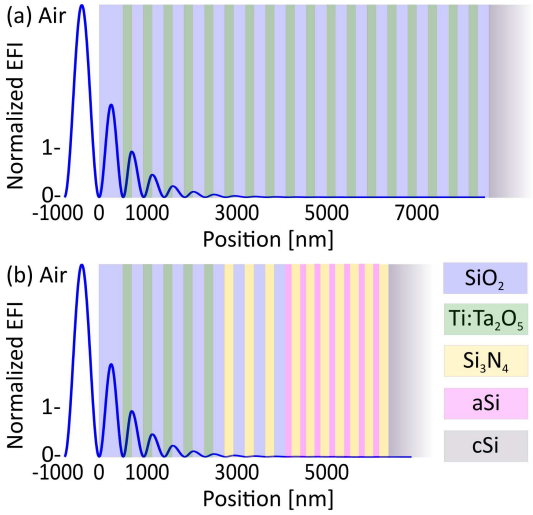

FIG. 7. (a) Schematic of a HR coating stack, which consists of 18 bilayers of SiO_2 (blue) and Ti:Ta_2O_5 (green) on a cSi (grey) substrate. The blue line shows the normalized electric field intensity (EFI) inside the coating. (b) Schematic of a four-material coating identical in reflectivity, in which the outermost 4 bilayers are made of SiO_2 and Ti:Ta_2O_5, while in the following 4 bilayers Ti:Ta_2O_5 is replaced by Si_3N_4 (yellow) as a high index material. The lowest 7 bilayers are made of Si_3N_4 and aSi (pink) with Si_3N_4 being the low index material.

while keeping thermal noise constant.

As the interferometrically sensed RPN spectral density is inversely proportional to the wavelength, the actual gain when changing from 1064 nm to 1550 nm is given by $\alpha_{1064}/\alpha_{1550} \times 1064\,\text{nm}/1550\,\text{nm} \approx 4.8$. Correspondingly, the gain with respect to the square root of the spectral density, for example calibrated to $\text{m}/\sqrt{\text{Hz}}$, is $\sqrt{4.8} = 2.2$.

B. Relevance for Coating Thermal Noise Reduction

HR coatings are based on alternating layers of two materials differing in refractive index n. In the simplest case, to achieve maximum reflectivity each layer has an optical thickness of $n \times t$ of a quarter of a wavelength, where t is the geometrical thickness. Figure 7 (a) shows a schematic of an HR coating stack, which consists of 18 bilayers of the materials currently used in GW detectors, SiO_2 (blue) and Ti:Ta_2O_5 (green), on a Si (pink) substrate resulting in a transmission of 6 ppm.

To reduce coating thermal noise, coating materials with low mechanical loss are required [30]. The mechanical loss of Si_3N_4 produced with LPCVD is $\phi = 8 \times 10^{-5}$ at room temperature and $\phi = 1 \times 10^{-5}$ at 20 K for a Si_3N_4 coating on a substrate [21], and even $\phi < 10^{-6}$ for highly stressed (≈ 1.2 GPa) substrate-free thin films [22]. For thermal noise calculations, the loss of LPCVD films measured on a substrate was used, as this case is better comparable to a GW detector mirror and the deposition method is the same as used for the membranes used for the absorption measurements.

Low optical absorption in the highly-reflective coatings is necessary to avoid thermal distortion of the test mass in a GW detector and, for cryogenic detectors, to maintain the low temperature. The optical absorption in a material is proportional to the integrated electric field (light) intensity (EFI). The blue line in Fig. 7 represents the electric field intensity EFI of the laser light in the coating. Due to etalon effects in thin films, the EFI in a multilayer coating is significantly different from the EFI in a thick (bulk) substrate scaled to identical thickness. The absorption measured on Si_3N_4 membranes in this work is about 1.0 /cm. Measuring at Brewster's angle without any etalon effects as occurring in thin films, this corresponds to the absorption coefficient in a bulk substrate.

To convert the absorption coefficient to the absorption in a HR coating composed of quarter layers, the absorption coefficient has to be scaled to the average EFI in a quarter layer. Figure 7(a) shows the EFI in a SiO_2/Ti:Ta_2O_5 multilayer stack which decreases by 50 % after each bilayer resulting in the sum of the EFI in all layers converging towards 2× the EFI in the first bilayer. The refractive index of Si_3N_4 is almost identical to Ti:Ta_2O_5 at 1550 nm making the EFI distribution in Fig. 7(a) representative for the following Si_3N_4 arguments.

Under the assumption that all the absorption takes place in the Si_3N_4 layers, the absorption of a quarter layer ($\lambda/4 \times 1/n$) of Si_3N_4 is $\alpha_{\text{QL}} = 1.0\,/\text{cm} \times 1550\,\text{nm}/(4 \times 2.17) \times 0.5 = 9\,\text{ppm}$, where the factor of 0.5 originates from the EFI in a QL in a SiO_2/Si_3N_4 coating being 0.5 × the full EFI without etalon effects (see previous paragraph). The absorption in a SiO_2/Si_3N_4 HR coating is $2 \times \alpha_{\text{QL}} = 18\,\text{ppm}$, which is too high for application in GW detectors, while the low mechanical loss makes Si_3N_4 still worth being considered as a coating material.

To enable using low loss materials with high optical absorption, the use of a coating design with more than two materials has been suggested [19, 20]. In this design, materials with low absorption are used in the outermost layers of the coating to reduce the laser power reaching the lower layers, while in the lower layers materials with higher absorption but lower mechanical loss can be used to reduce thermal noise.

A three-material coating made of 8 bilayers of SiO_2 and Ti:Ta_2O_5 on top of 4 bilayers of SiO_2 and amorphous silicon (aSi) was proposed in [19]. A pure SiO_2 and aSi HR coating would absorb 1000 ppm at 1550 nm [31, 32]. After 8 bilayers of SiO_2 and Ti:Ta_2O_5 only 0.34 % of the input laser power are left and the part of the coating containing aSi would only contribute 3.4 ppm to the total coating absorption (assuming the absorption of SiO_2 to be negligible). Replacing the lower 10 bilayers of SiO_2 and Ti:Ta_2O_5 by 4 bilayers of SiO_2 and aSi results in the same reflectivity as 18 bilayers of SiO_2 and Ti:Ta_2O_5, because of the much higher refractive index of aSi ($n = 3.5$) compared to Ti:Ta_2O_5 ($n = 2.05$). The reduced number

	loss ϕ $\times 10^{-4}$				Young's modulus [GPa]				Brownian th. noise (100 Hz) $\times 10^{-21}$ [m/$\sqrt{Hz}$]		
	SiO_2	aSi	$Ti:Ta_2O_5$	Si_3N_4	SiO_2	aSi	$Ti:Ta_2O_5$	Si_3N_4	$SiO_2/Ti:Ta_2O_5$	multi mat.	(improvement)
290 K	0.4 [33]	1.0 [34]	2.3 [33]	0.8 [21]					2.90	2.07	(29 %)
120 K	1.7 [35]	0.8 [34]	3.3 [36]	0.2 [21]	72 [38]	147 [37]	140 [38]	270 [26]	2.74	1.66	(39 %)
20 K	7.8 [35]	0.2 [34]	8.6 [36]	0.1 [21]					2.13	1.26	(41 %)

TABLE III. Loss ϕ at room temperature (RT), 120 K and 20 K and Young's modulus at all temperatures and used for calculating the resulting Brownian thermal noise for 18 bilayers of SiO_2 and $Ti:Ta_2O_5$, and for a multimaterial coating as shown in 7(b).

of bilayers reduces coating thermal noise at room temperature by approximately 20 % in this design. At low temperatures the mechanical loss of aSi is significantly lower than the loss of $Ti:Ta_2O_5$ resulting in a total thermal noise reduction of approximately 25 % at 20 K.

Based on a coating absorption of 18 ppm, for a wavelength of 1550 nm after 5 bilayers of SiO_2 and $Ti:Ta_2O_5$ the absorption contribution of Si_3N_4 would be reduced to $(0.5)^5 \times 18\,\text{ppm} < 1\,\text{ppm}$. Figure 7 (b) shows a schematic of a four-material coating identical in reflectivity to (a), in which the outermost 5 bilayers are made of SiO_2 and $Ti:Ta_2O_5$, while in following 3 bilayers $Ti:Ta_2O_5$ is replaced by Si_3N_4 (yellow) as a high index material. The lowest 7 bilayers are made of Si_3N_4 and aSi (pink) with Si_3N_4 being the low index material. Table III presents the resulting thermal noise at room temperature, 120 K and 20 K for 18 bilayers of SiO_2 and $Ti:Ta_2O_5$ and the possible improvement using the multimaterial coating with aSi and Si_3N_4 showing a thermal noise improvement of up to 41 % at 20 K. In the case of a decrease in absorption with temperature, more $Ti:Ta_2O_5$ layers could be replaced by Si_3N_4 and the thermal noise improvement would increase. The loss and Young's modulus used for the calculations are also shown in Tab. III. As the total thermal noise of this coating design is dominated by the loss of the SiO_2 and $Ti:Ta_2O_5$ layers, a 10× lower loss of high-stress Si_3N_4 would change the total coating thermal noise at 20 K by less than 1 %. All calculations are made for coating on a silicon substrate and for a laser beam radius of 9 cm.

V. CONCLUSION

A possible approach for improving GW detectors is using crystalline silicon, which shows low thermal noise at low temperatures and a low optical absorption at 1550 nm, as a test-mass material.

We have shown that a wavelength of 1550 nm is also superior to 1064 nm for RPN experiments using Si_3N_4 membranes. Measurements on low stress membranes have shown an absorption decrease by a factor of about 7 at 1550 nm. While it seems unlikely that the absorption ratio between the two wavelengths changes with stress, the effect of stress on the optical absorption of membranes is worth investigation.

Extending absorption measurements to silicon nitride films of different stoichiometry (and thus different refractive index) is also of interest, in particular for potential designs using different compositions of SiN_x for both the high and low-index coating layers [17].

The measured absorption of 1.0 /cm resulting in a coating absorption of 18 ppm for a SiO_2/Si_3N_4 multilayer coating makes Si_3N_4 (combined with SiO_2) an interesting alternative material for $Ti:Ta_2O_5$ in upper layers and for SiO_2 (combined with Si) in lower layers of multimaterial coatings. This would enable a 41 % improvement in thermal noise at 20 K compared to a pure $SiO_2/Ti:Ta_2O_5$ coating.

APPENDIX A

Transmission of a Membrane

For calculating the angle of total transmission for the membrane geometrical effects have to be considered. Figure 8 shows a schematic of the membrane (yellow) and the laser beam (red). To calculate the reflected field, the optical path difference of the beam reflected at the membrane surface (1) and the beam reflected at the membrane back side (2) has to be calculated, which is

$$\Delta p = n_2 \times (AB + BC) - n_1 \times AP = 2\, n_2\, \mathrm{d}/\cos\beta - \mathrm{AP} \quad (3)$$

for n_1=1 and AB=BC=d/cosβ. At P, the angle is 90° so that sinα=AP/AC. The distance AC can be expressed as 2d× tanβ giving

$$\Delta p = 2\, n_2\, \mathrm{d}/\cos\beta - 2\mathrm{d}\tan(\beta)\sin(\alpha)\,. \quad (4)$$

By using Snell's law, $n_1 \sin(\alpha) = n_2 \sin(\beta)$, Eq. 4 can be written as

$$\Delta p = 2\,\mathrm{d}\,\sqrt{n_2^2 - \sin^2\alpha}\,. \quad (5)$$

For reflection at A where $n_1 < n_2$, the light field gets an additional phase shift of π resulting in a change of Δ p by $\lambda/2$, while at B no additional phase shift is induced as $n_2 > n_1$, resulting in

$$\Delta p = 2\,\mathrm{d}\,\sqrt{n^2 - \sin^2\alpha} - \lambda/2\,. \quad (6)$$

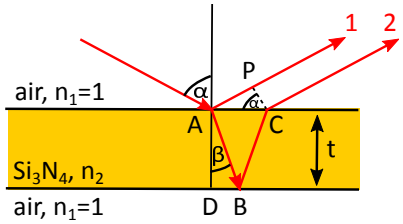

FIG. 8. Schematic of the Si_3N_4 membrane (yellows) and the incident and reflected laser beams (red).

To maximize the transmission of the membrane, the reflected light field has to minimize requiring destructive interference of the beams 1 and 2 which is given for Δ p = (k + 1/2)λ with k $\in \{0, 1, 2, ...\}$.

From these relationships an angle of maximum transmission of

$$\alpha = \arcsin\sqrt{\mathrm{n}^2 - \left(\frac{\mathrm{k}+1}{2\mathrm{d}}\lambda\right)^2} \tag{7}$$

results. As arcsin(x) is only defined for $-1 \leq x \leq 1$, two restrictions follow on the expression in the square root in Eq. 7, which are

$$n^2 - \left(\frac{k+1}{2d}\lambda\right)^2 \leq 1 \quad \text{and} \quad n \geq \frac{k+1}{2d}\lambda\,. \tag{8}$$

From Eqs. 8, for the different membrane thicknesses the following restrictions on k result,

$$\begin{aligned} 3.74 \leq k_{2\mu\mathrm{m}} &\leq 4.33\,, \\ 1.39 \leq k_{1\mu\mathrm{m}} &\leq 1.69\,, \\ 0.19 \leq k_{500\mathrm{nm}} &\leq 0.34\,, \\ &\ldots \end{aligned} \tag{9}$$

which show that 2 μm is the thinnest of the membranes available for which a k $\in \{0, 1, 2, ...\}$ exists. For a 2 μm and k=4, from Eq. 7 results an angle of incidence of $\alpha = 51.3°$.

ACKNOWLEDGEMENTS

We acknowledge support from the SFB/Transregio 7, the International Max Planck Research School (IMPRS) on Gravitational Wave Astronomy, and from QUEST, the centre for Quantum Engineering and Space-Time Research. We are grateful for additional financial support from the Royal Society (RG110331), STFC and the University of Glasgow. IWM is supported by a Royal Society Research Fellowship. SR holds a Royal Society Wolfson Research Merit award. We are grateful to the International Max Planck Partnership for Measurement and Observation at the Quantum Limit for support, and we thank our colleagues in the LSC and VIRGO collaborations and within SUPA for their interest in this work. SS acknowledges support by the Alexander von Humboldt foundation and the European Commission H2020-MSCA-IF-2014, grant agreement 658366. This research has been supported by the ERC project MassQ (grant agreement number 339897).

This paper has LIGO Document number LIGO-P1600343.

[1] B. P. Abbott et al., Observation of Gravitational Waves from a Binary Black Hole Merger, Phys. Rev. Lett. 116, 061102 (2016)

[2] G. M. Harry Advanced LIGO: the next generation of gravitational wave detectors, Classical and Quantum Gravity 8, 084006 (2010)

[3] T. P. Purdy, R. W. Peterson, C. A. Regal, Observation of Radiation Pressure Shot Noise on a Macroscopic Object, *Science* **339**, 6121, pp. 801–804 (2013)

[4] P. Verlot, A. Tavernarakis, T. Briant, P.-F. Cohadon, A. Heidmann, Scheme to probe optomechanical correlations between two optical beams down to the quantum level, *Phys. Rev. Lett.* **102**, 103601 (2009)

[5] K. Borkje, A. Nunnenkamp, B. M. Zwickl, C. Yang, J. G. E. Harris, and S. M. Girvin, Observability of radiation–pressure shot noise in optomechanical systems, *Phys. Rev. A* **82**, 013818 (2010)

[6] D. Friedrich, H. Kaufer, T. Westphal, K. Yamamoto, A. Sawadsky, F. Khalili, S. L. Danilishin, S. Goler, K. Danzmann, and R. Schnabel, Laser interferometry with translucent and absorbing mechanical oscillators, *New Journal of Physics* **13**, 093017 (2011)

[7] A. Sawadsky, H. Kaufer, R. Moghadas Nia, S. P. Tarabrin, F. Y. Khalili, K. Hammerer, and R. Schnabel, Observation of Generalized Optomechanical Coupling and Cooling on Cavity Resonance, *Phys. Rev. Lett.* **114**, 043601 (2015)

[8] A. M. Jayich, J. C. Sankey, B. M. Zwickl, C. Yang, J. D. Thompson, S. M. Girvin, A. A. Clerk, F. Marquardt, and J. G. E. Harris, Dispersive Optomechanics: A Membrane Inside a Cavity, *New Journal of Physics* **10**, 095008 (2008)

[9] R. Adhikari et al., LIGO III Blue ConceptLIGO, Technical Document LIGO-G1200573, dcc.ligo.org/LIGO-G1200573-v1/public (2012)

[10] M. Abernathy et al., Einstein gravitational wave Telescope (ET) conceptual design study, ET-0106C-10, https://tds.ego-gw.it/ql/?c=7954 (2011)

[11] S. Hild, S. Chelkowski, A. Freise, J. Franc, N. Morgado, R. Flaminio, and R. DeSalvo, A xylophone configuration for a third–generation gravitational wave detector, *Classical Quantum Gravity* **27**, 015003 (2010)

[12] M. E. Fine, H. Van Duyne, and N. T. Kenney, LowTemperature Internal Friction and Elasticity Effects in Vitreous Silica, *J. Appl. Phys.* **25**, 402 (1954)

[13] D. F. McGuigan, C. C. Lam, R. Q. Gram, A. W. Hoffman, D. H. Douglass, and H. W. Gutche, Measurements of the mechanical Q of single-crystal silicon at low temperatures, *Journal of Low Temperature Physics* **30** 621–629 (1978)

[14] W. Winkler, K. Danzmann, A. Rüdiger, and R. Schilling, Heating by optical absorption and the performance of interferometric gravitational-wave detectors, *Physical Review A* **44**, 7022, (1991)

[15] I. W. Martin et al., Low temperature mechanical dissipation of an ion-beam sputtered silica film, *Classical Quantum Gravity* **31**, 035019 (2014)

[16] I. W. Martin et al., Comparison of the temperature dependence of the mechanical dissipation in thin films of Ta_2O_5 and Ta_2O_5 doped with TiO_2, *Classical Quantum Gravity* **26**, 155012 (2009)

[17] S. Chao, H. Pan, L. Kuo, S. Huang, M. Wu, Y. Juang, and C. Lee, Silicon-nitride Films Deposited by PECVD Method on Silicon Substrate for Next Generation Laser Interference Gravitational Wave Detector, in Optical Interference Coatings 2016, OSA Technical Digest (online) (Optical Society of America, 2016), paper MB.12

[18] L. Kuo, H. Pan, C. Lin, and S. Chao Cryogenic Losses for Titania, Silica, Silicon Nitride Films and Silicon Substrates LIGO Technical Document LIGO-G1601703,

[19] J. Steinlechner, I. W. Martin, C. Krueger, J. Hough, S. Rowan, and R. Schnabel, Thermal Noise Reduction and Absorption Optimisation via Multi-Material Coatings, *Phys. Rev. D* **91**, 042001 (2015)

[20] W. Yam, S. Gras, and M. Evans, Multimaterial coatings with reduced thermal, *Phys. Rev. D* **91**, 042002 (2015)

[21] X. Liu, T. H. Metcalf, Q. Wang, and D. M. Photiadis, in Proceedings of Symposium A: Amorphous and Polycrystalline Thin-Film Silicon Science and Technology, Elastic Properties of Several Silicon Nitride Films, 2007 (MRS, Pittsburgh, PA, 2007), Vol. 989, p. 511.

[22] D. R. Southworth, R. A. Barton, S. S. Verbridge, B. Ilic, A. D. Fefferman, H. G. Craighead, and J. M. Parpia, Stress and Silicon Nitride: A Crack in the Universal Dissipation of Glasses, *Phys. Rev. Lett.* **102**, 225503 (2009)

[23] A. L. Alexandrovski, M. M. Fejer, A. Markosyan, and R. Route, Photothermal common-path interferometry (PCI): new developments, Proc. SPIE 7193, Solid State Lasers XVIII: Technology and Devices **71930D** doi: 10.1117/12.814813 (2009)

[24] V. Raghunathan, W. N. Ye, J. Hu, T. Izuhara, J. Michel, and L. Kimerling, Athermal operation of Silicon waveguides: spectral, second order and footprint dependencies, *Optics Express* **18**, pp. 17631–17639 (2010)

[25] http://www.azom.com/properties.aspx?ArticleID=53

[26] Norcada Inc., Canada, www.norcada.com

[27] A. Jain, and K. E. Goodson, Measurement of the Thermal Conductivity and Heat Capacity of Free-Standing Shape Memory Thin Films using the 3w Method, *ASME Journal of Heat Transfer* **130**, 102402 (2008)

[28] N. Lastzka, J. Steinlechner, S. Steinlechner, and R. Schnabel, Measuring small absorptions by exploiting photothermal self-phase modulation, *Applied Optics* **49**, 5391–5398 (2010)

[29] E. D. Black, An introduction to PoundDreverHall laser frequency stabilization, *Am. J. Phys.* **69** 79 – 87 (2001)

[30] G. M. Harry et al., Thermal noise in interferometric gravitational wave detectors due to dielectric optical coatings, Class. Quantum Grav. **19**, 897–917 (2002)

[31] J. Steinlechner, A. Khalaidovski, R. Schnabel, Optical absorption measurement at 1550 nm on a highly-reflective Si/SiO_2 coating stack, *Class. Quantum Grav.* **31**, 105005 (2014)

[32] J. Steinlechner, I. W. Martin, R. Bassiri, A. Bell, M. M. Fejer, J. Hough, A. Markosyan, R. K. Route, S. Rowan, Z. Tornasi, Optical Absorption of Ion-Beam Sputtered aSi Coatings, *Phys. Rev. D* **93** 062005, 2016

[33] R. Flaminio, J. Franc, C. Michel, N. Morgado, L. Pinard, and B. Sassolas, A study of coating mechanical and optical losses in view of reducing mirror thermal noise in gravitational wave detectors, *Class. Quantum Grav.* **27**, 084030 (2010)

[34] P. G. Murray, I. W. Martin, K. Craig, J. Hough, R. Robie, S. Rowan, M. R. Abernathy, T. Pershing, and S. Penn, Ion-beam sputtered amorphous silicon films for cryogenic precision measurement systems, *Phys. Rev. D* **92**, 062001 (2015)

[35] I. W. Martin, R. Nawrodt, K. Craig, C. Schwarz, R. Bassiri, G. Harry, J. Hough, S. Penn, S. Reid, R. Robie, and S. Rowan, Low temperature mechanical dissipation of an ion-beam sputtered silica film, *Class. Quantum Grav.* **31**, 035019 (2014)

[36] I. W. Martin et al., Effect of heat treatment on mechanical dissipation in Ta_2O_5 coatings, *Class. Quantum Grav.* **27**, 225020 (2010)

[37] M. R. Abernathy, Ph.D. thesis, University of Glasgow, 2012

[38] M. M. Fejer, S. Rowan, G. Cagnoli, D. R. M. Crooks, A. Gretarsson, G. M. Harry, J. Hough, S. D. Penn, P. H. Sneddon, and S. P. Vyatchanin, Thermoelastic dissipation in inhomogeneous media: loss measurements and displacement noise in coated test masses for interferometric gravitational wave detectors, *Phys. Rev. D* **70**, 082003, 2004